Ultra-low coercive field of improper ferroelectric $Ca_3Ti_2O_7$ epitaxial thin films ⓕ

X. Li ⓘᴰ, L. Yang, C. F. Li, M. F. Liu, Z. Fan, Y. L. Xie, C. L. Lu, L. Lin, Z. B. Yan, Z. Zhang, J. Y. Dai, J.-M. Liu ⓘᴰ, and S. W. Cheong

COLLECTIONS

ⓕ   This paper was selected as Featured

View Online   Export Citation   CrossMark

ARTICLES YOU MAY BE INTERESTED IN

Interrelation between domain structures and polarization switching in hybrid improper ferroelectric $Ca_3(Mn,Ti)_2O_7$
Applied Physics Letters **110**, 222906 (2017); https://doi.org/10.1063/1.4984841

Hybrid improper ferroelectricity in Ruddlesden-Popper $Ca_3(Ti,Mn)_2O_7$ ceramics
Applied Physics Letters **106**, 202903 (2015); https://doi.org/10.1063/1.4921624

Optical spectroscopy and band gap analysis of hybrid improper ferroelectric $Ca_3Ti_2O_7$
Applied Physics Letters **108**, 262901 (2016); https://doi.org/10.1063/1.4954404

Ultra-low coercive field of improper ferroelectric Ca₃Ti₂O₇ epitaxial thin films

X. Li,[1,a)] L. Yang,[2] C. F. Li,[1] M. F. Liu,[1] Z. Fan,[2] Y. L. Xie,[1] C. L. Lu,[3,a)] L. Lin,[1] Z. B. Yan,[1] Z. Zhang,[4] J. Y. Dai,[4] J.-M. Liu,[1,2] and S. W. Cheong[5]

[1]*Laboratory of Solid State Microstructures and Innovative Center of Advanced Microstructures, Nanjing University, Nanjing 210093, China*
[2]*Institute for Advanced Materials, South China Normal University, Guangzhou 510006, China*
[3]*School of Physics, Huazhong University of Science and Technology, Wuhan 430074, China*
[4]*Department of Applied Physics, Hong Kong Polytechnic University, Hong Kong, China*
[5]*Rutgers Center for Emergent Materials and Department of Physics and Astronomy, Rutgers University, Piscataway, New Jersey 08854, USA*

Hybrid improper ferroelectrics have their electric polarization generated by two or more combined non-ferroelectric structural distortions, such as the rotation and tilting of Ti-O octahedral in the Ca₃Ti₂O₇ (CTO) family. In this work, we prepare the high quality (010)-oriented CTO thin films on (110) SrTiO₃ (STO) substrates by pulsed laser deposition. The good epitaxial growth of the CTO thin films on the substrates with the interfacial epitaxial relationship of [001]CTO//[001]STO and [100]CTO//[-110]STO is revealed. The in-plane ferroelectric hysteresis unveils an ultralow coercive field of ∼5 kV/cm even at low temperature, nearly two orders of magnitude lower than that of bulk CTO single crystals. The huge difference between the epitaxial thin films and bulk crystals is most likely due to the lattice imperfections in the thin films rather than substrate induced lattice strains, suggesting high sensitivity of the ferroelectric properties to lattice defects. *Published by AIP Publishing.* [http://dx.doi.org/10.1063/1.4974217]

Ferroelectrics and the underlying mechanisms have undergone a rapid revival in recent years due to the discovery of a series of emergent phenomena on one hand and promising applications in the next generation of data storages and spintronics on the other hand.[1,2] Two parallel roadmaps have been proceeding. One roadmap goes ahead by down-scaling ferroelectrics into nanostructures. This in turn stimulates interest in the dynamics of domain walls and new polar structures.[3] The other roadmap, much broader and more attractive, is to search for novel ferroelectrics and multiferroics as an extended discipline of correlated electronic physics and materials science. The magnetoelectric (ME) coupling associated with multiferroicity was once placed high expectation to functionalize the electro-control of magnetism with ultralow power consumption.[4,5] While the second roadmap has made substantial progress, some major issues remain. In 2011, Fennie and colleagues predicted hybrid improper ferroelectricity in 327 Ruddlesden-Popper layered A₃B₂O₇ compounds[6] and the controls of both ferromagnetism and ferroelectricity in the magnetic compound Ca₃Mn₂O₇.[7–10] So far, such a prediction has not yet been confirmed experimentally, and nevertheless, the 327-type ferroic oxides have again come to researchers' vision.[11]

In fact, some hybrid improper ferroelectrics as a subclass of geometric ferroelectrics have been known.[12] The electric polarization P is generated via a collective distortion of non-ferroelectric structural order parameters.[6,9,13] Ca₃Ti₂O₇ (CTO) and similar A₃B₂O₇ titanates belong to this subclass. The CTO lattice, as shown in Fig. 1(a), exhibits the $A2_1am$ space group and orthorhombic structure at room temperature

with lattice constants $a = 5.423$ Å, $b = 5.417$ Å, and $c = 19.417$ Å.[14] The collective distortion of TiO₆ octahedral rotation around the c-axis and tilting around the a-axis allows the net displacement of the A-site ions along the a direction, leading to the net polarization, as shown in Fig. 1(b). To get a straightforward view of the epitaxy with some substrates, a pseudo-tetragonal lattice is also labeled as [100]ₚₜ and [010]ₚₜ, as shown in Fig. 1(c), which have a 45° rotation relative to the orthorhombic a- and b-axes of CTO, respectively.

The ferroelectricity in CTO-based systems has not been confirmed until recently, probably due to either the large coercive field or lattice imperfections.[6] A prominent progress is the observations of well-defined ferroelectric hysteresis
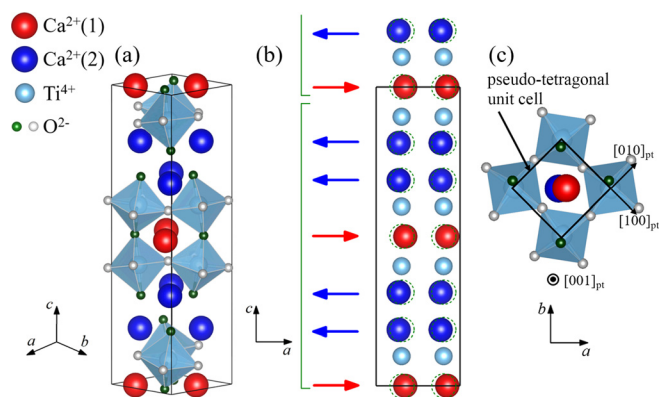
FIG. 1. (a) Crystal structure of CTO with the $A2_1am$ space group. (b) The proposed ionic displacements for ferroelectric polarization of CTO, represented by the arrows pointing from ions' initial positions (green dashed circles) for each Ca²⁺ layer. (c) The relationship between the axes of $A2_1am$ and its pseudo-tetragonal unit cell. The black square line represents the CTO pseudo-tetragonal unit cell with arrows pointing out the directions. Both c-axes (or [001] direction) are perpendicular to the screen.

a)Electronic addresses: lixplus@126.com and cllu@mail.hust.edu.cn

and rich domain structure in CTO single crystals.[15,16] Ferroelectricity and weak ferromagnetism were found in $(Ca_ySr_{1-y})_{1.15}Tb_{1.85}Fe_2O_7$-CTO[17] where the strong ME control and ferroelectric hysteresis remain to be confirmed. Even though the coercive field of $(Ca,Sr)_3Ti_2O_7$ is as high as ~130 kV/cm, the first-principles calculations predicted that coercive field is even much higher. Such a high coercive field hinders substantially potential applications of these novel ferroelectrics. In addition, the collective distortion rather than a single distortion induced polarization would make the ferroelectricity sensitive to intrinsic/external perturbations such as lattice strain and imperfections.[18] A recent theoretical prediction revealed the polar-nonpolar transition driven by a relatively small lattice strain.[19]

Our main motivation is to explore the ferroelectricity of the CTO thin films and its possible difference from the bulk single crystals. On one hand, preparation of high quality films is the pre-requisite for practical applications.[20–22] On the other hand, checking the CTO thin films may provide additional knowledge on the microstructure-property relationship for hybrid ferroelectrics, in particular, on how to reduce the reported high coercive field for polarization switching. It comes to us that the best lattice match can be between the CTO (010) plane and the cubic $SrTiO_3$ (STO) (110) plane ($a = 3.905$ Å), with a slight in-plane tension strain and weak out-of-plane contraction. The proposed epitaxy is shown in Fig. 2(a) where five unit periods of STO along the [001]-axis match well with one unit period on CTO along the c-axis, leading to epitaxial relationships of [001]CTO//[001]STO and [100]CTO//[−110]STO. In addition, two issues should be addressed. First, given the a-axis polarization, a slight in-plane tension strain may anyway affect the ferroelectricity including the polarization and coercive field. Second, for thin films, lattice imperfections exist inevitably allowing opportunity to check the sensitivity of ferroelectricity, e.g., the coercive field E_c, to these defects.

A brief description of the CTO film deposition on (110) STO substrates using pulsed laser deposition and property characterizations is presented in the supplementary material. For typical cases, the thin films are ~60 nm in thickness. For electric characterization, the gold inter-digital surface electrodes were sputtered via the standard photolithography and lift-off procedures.[23,24] The room-temperature X-ray diffraction (XRD) θ–2θ spectrum of one as-prepared sample is plotted in Fig. 2(b) where only the CTO (010) and STO (110) reflections can be detected. The full-widths at the half-height (FWHH) of the CTO peaks are comparable with those of the STO peaks. For the epitaxy identification, one performed the XRD ϕ-scan on the CTO (115) and STO (111) reflections, as shown in Figs. 2(c) and 2(d). The four sharp CTO (115) reflections with the inter-peak separations of 70.6° and 109.4°, respectively, are probed, consistent with the calculated values of 71.2° and 108.8°. The inter-angle of 70.6° between two (115) peaks is symmetrically divided by the STO (111) peak, confirming that the in-plane lattice of CTO thin film does match epitaxially with the substrate via the [100]CTO//[-110]STO and [001]CTO//[001]STO alignment.

We discuss the lattice distortion of the thin films. The orthorhombic unit of CTO is grown on a ($3.905 \times \sqrt{2}$ Å) $\times$ (3.905×5 Å) rectangular STO lattice (Fig. 2(a)). The

FIG. 2. (a) The proposed in-plane epitaxial relationships across the CTO and STO interface: [001]CTO//[001]STO and [100]CTO//[-110]STO. (b) X-ray θ–2θ spectrum for the CTO film grown on the (110)STO substrate. (c) In-plane projections of the vectors perpendicular to the CTO (115) and STO (111) reflections. (d) The XRD ϕ-scans of the CTO (115) (red line) and STO (111) (black line) reflections.
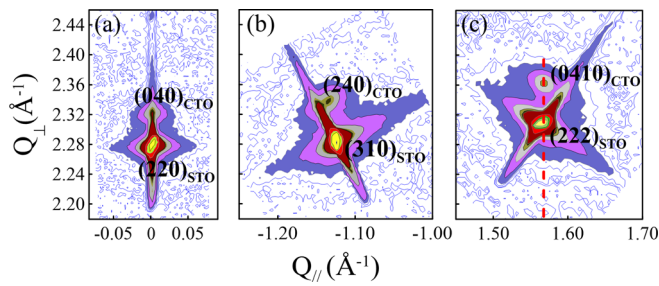
FIG. 3. The measured RSM images of the CTO film on the STO substrate: (a) the symmetric STO (220) and CTO (040) reflections; (b) the asymmetric STO (310) and CTO (240); and (c) the asymmetric STO (222) and CTO (0 4 10).

interfacial lattice misfit is only 1.0% along the *a*-axis and 0.6% along the *c*-axis, and the strain inside the film far from the interface is slightly smaller, as confirmed by the XRD data. Besides, the symmetric and asymmetric XRD reciprocal space mapping (RSM) results are presented in Figs. 3(a)–3(c), respectively. For the symmetric STO (220) and CTO (040) reflections, the CTO (040) spot exhibits some broadening along wavevector $Q_\perp$, implying a slight variation in lattice constant *b*. The broadening along the wavevector $Q_{//}$ suggests a consistent FWHH with the direct rocking curve. Fig. 3(b) gives the asymmetric STO (310) and CTO (240) reflections, with wavevector $Q_{//}$ parallel to the *a*-axis of CTO. The lattice along the *a*-axis is partially relaxed. Fig. 3(c) gives the asymmetric STO (222) and CTO (0 4 10) reflections, with wavevector $Q_{//}$ parallel to the *c*-axis of CTO. As indicated by the red dashed line, the lattice of the CTO film along the *c*-axis is coherent with the STO. The RSM images reveal a clear pattern from all the directions including the (*a*, *b*, *c*)-axes of the CTO film.

The transmission electron microscopy (TEM) images across the CTO-STO interface are summarized in Fig. 4. The low-amplified image reveals the microstructural homogeneity over a big scale. The selected area electron diffraction

(SAED) pattern along the [001] axis of CTO and STO in Fig. 4(b) confirms the out-of-plane (020)CTO//(110)STO and in-plane (200)CTO//(1–10)STO relationships. The spots from the CTO are much weaker than those from STO, suggesting the relatively high density of lattice imperfections in the CTO. A relatively detailed discussion on the possible lattice defects in the CTO thin films is given in the supplementary material (Figs. S1 and S2), suggesting the interstitial and vacancy defects in the films. Near the interface, the CTO *b*-axis lattice constant is 5.402 Å, twice of the Ca-Ca distance 2.701 Å. The *a*-axis lattice constant is 5.516 Å, twice of the Ca-Ca distance 2.758 Å. The *a*-axis constant in this region is larger than that of the bulk crystal, whereas the *b*-axis constant is smaller, confirming the slight in-plane tension and out-of-plane contract. Towards the region far from the interface, the *b*-axis and *a*-axis constants are 5.416 Å and 5.496 Å (twice of the Ca-Ca distances 2.708 Å and 2.748 Å, respectively), close to the bulk crystal values, indicating the gradual lattice relaxation of the film, as schematically drawn in Fig. 4(d). This relaxation can be also detected by the spot splitting in the SAED pattern where the CTO (260) and STO (420) are no longer overlapped but in two separated spots.

The positive-up and negative-down (PUND) method was used to measure the total electric current (*J*) across the two sets of electrode stripes, as shown in the supplementary material (Fig. S3) where several sets of *J-E* data at $T = 2$ K with the *E*//*a*-axis and relevant discussion are presented. It is noted that the data by the PUND measurement at room temperature are unreliable due to the large electric leakage, and here, we present the data at low temperature. Based on these *J-E* data, one evaluates the *P-E* loops at different *E*-amplitudes (E_0), and the representative results are summarized in Fig. 5(a). First, the well-developed loops are identified at low temperature, and the measured "maximum" polarization increases with increasing E_0. The remnant polarization is ~ 8 μC/cm^2 at $E_0 = 20$ kV/cm on the same order of magnitude as the bulk single crystals.[15] Second, in spite of
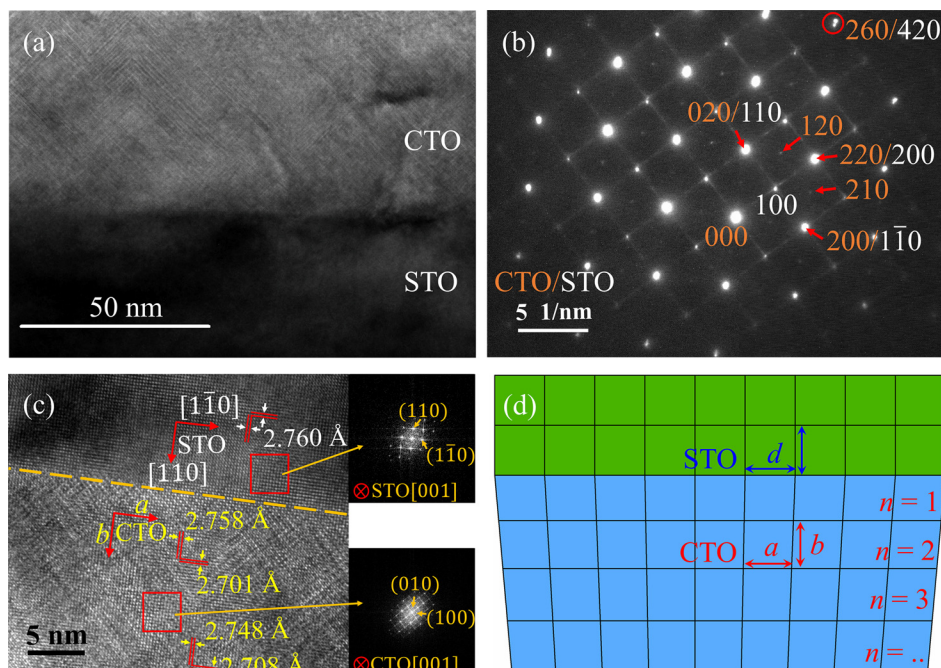

FIG. 4. (a) The TEM image showing the CTO film on the STO substrate. (b) The SAED pattern along the [001] axis of CTO. The orange and white colored numbers represent the spots of CTO and STO, respectively. (c) Cross-section TEM image of the CTO film around the CTO/STO interface. The insets represent the fast Fourier transform patterns from the selected areas. (d) An enlarged relaxation schematic of lattice relaxation.
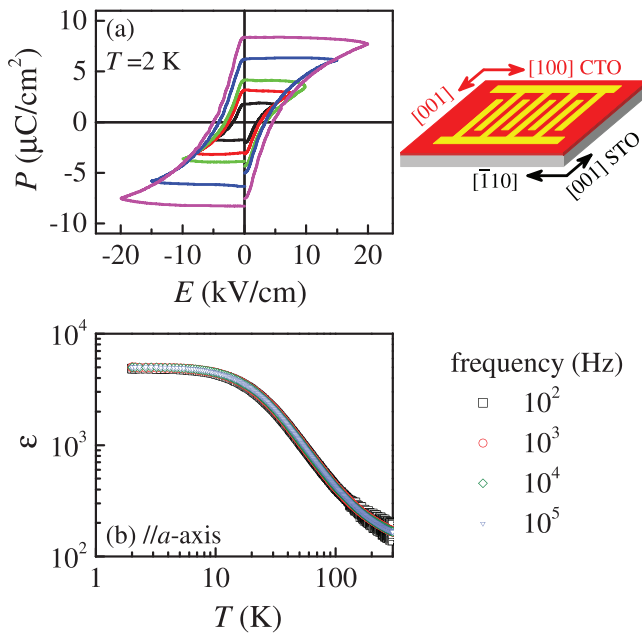
FIG. 5. Ferroelectric hysteresis loop measured along the *a*-axis of CTO using the PUND method: (a) loops with different *E*-amplitudes (E_0) at $T = 2$ K. The schematic of the sample with inter-digital electrodes is displayed on the top right. (b) Measured dielectric constant $\varepsilon(T)$ curves along the *a*-axis at several frequencies in the log-log scale.

E_0-dependence, the measured coercive field (E_c) is 2.0 kV/cm–5.0 kV/cm, dependent of E_0 but much lower than that (>100 kV/cm) for bulk single crystals. In the other words, the ferroelectricity in the CTO thin films seems to be very different from the bulk single crystal. While the remnant polarization remains nearly the same as the bulk system, the coercive field is dramatically reduced, favorable for practical applications.

Besides, we measured the dielectric constant ε as a function of temperature *T*, and the $\varepsilon(T)$ curves at several frequencies are plotted in Fig. 5(b). We see a monotonous increasing of ε with decreasing *T* till $T \sim 10$ K below which a dielectric plateau is identified. In the log-log scale, one observes no any anomaly over the whole *T*-range, suggesting no ferroelectric transition below room temperature, similar to the bulk system whose transition temperature is far above room temperature. Here, several facts deserve to be mentioned. First, the typical quantum paraelectric behavior in terms of the dielectric response at low *T* is identified, suggesting that the major dielectric response is from the underlying STO. Second, no frequency dispersion of the dielectric response in the covered frequency range implies the same consequence. Third, this trivial quantum paraelectric behavior implies that the surface layer of STO is not affected by the interfacial lattice mismatch, and the measured polarization comes from the CTO film. Fourth and more importantly, for our PUND measurements, the underlying STO of high dielectric constant at low *T* may possibly disturb the electric potential distribution during the PUND probing, making the coercive field data inaccurate. Here, we prepared a set of CTO films with different thicknesses to verify our calculation of the coercive field. The experimental results prove that the evaluated coercive field is indeed the actual coercive field of the film, and detailed discussion can be found in the supplementary material (Figs. S4 and S5).

To this stage, one concludes that the CTO thin films in the present condition have their ferroelectric polarization comparable with the bulk single crystals but with much lower coercive field E_c for polarization switching. The reasons for the big differences can be complicated. The lattice strain, defect state, domain structure, and dimensionality-relevant consequences can account for the big differences, considering the rich domain structure and the prediction that lattice strain may suppress the ferroelectricity.[16,19,25] Here, the lattice strain effect should be checked carefully, and we consult to the first principles calculations while the others remain open for a satisfactory understanding. We employ the first-principles calculations based on the projected augmented wave (PAW) pseudo-potentials using the Vienna *Ab-initio* Simulation Package (VASP). More details of the calculation procedure are given in the supplementary material, and the results are reported there too (Fig. S6). For the bulk lattice, we discuss the initial state (A2$_1$am), intermediate state (Pbcn), and final state (A2$_1$am). The fully relaxed lattice constants for the A2$_1$am ferroelectric phase are $a = 5.442$ Å, $b = 5.393$ Å, and $c = 19.336$ Å, with a unit volume of 567.53 Å^3.[14] The evaluated polarization *P* is ~ 12.9 μC/cm^2, consistent with measured polarization at room temperature.[15] The energy barrier for polarization switching is ~ 31 meV/Ti, giving an equivalent coercive field of ~ 3000 kV/cm at near zero-temperature if $P = 20$ μC/cm^2. This value is one order of magnitude larger than the room-temperature value.[26] For the CTO thin films, the lattice relaxation is performed by fixing lattice constants $a = 5.522$ Å and $c = 19.525$ Å as determined from the in-plane lattices of the (110)STO substrate. Again, the Pbcn state is chosen as the intermediate switching state. The barrier for the switching is ~ 43 meV/Ti, slightly larger than that of the bulk crystal. The *a*-axis polarization is 17.6 μC/cm^2, and the volume is 575.34 Å^3. These calculations suggest that the lattice tension induced by the STO substrates may not be the main reason for the huge difference in the coercive field between the bulk and thin films.

Other possible reasons for such a difference come from the lattice imperfections in the thin films, including the lattice defects (Fig. S2, supplementary material), domain structures, and possible non-stoichiometry. Again, it is mentioned that the hybrid improper ferroelectricity in CTO is the consequence of collective distortion of oxygen octahedral rotation and tilting. The local lattice defects can be vital for ferroelectric ordering. In addition, the CTO single crystals have complicated domain patterns with high domain wall energy due to the high density of head-to-head and tail-to-tail walls. The domain structures in thin films of high density of lattice imperfections can be more complicated, probably allowing the low coercive field for polarization switching. Details of the physics remain open to us at this stage.

In conclusion, we have prepared high-quality epitaxial CTO thin films on (110) STO substrates. A series of micro-structural characterizations have been presented, identifying the epitaxial relationship of [001]CTO//[001]STO and [100]CTO//[-110]STO. The measurements reveal that the ferroelectric polarization aligns along the in-plane *a*-axis, and extra-high coercive field in the bulk single crystals can be markedly reduced down to ~ 5 kV/cm. The first principles calculations suggest that the in-plane tension and out-of-plane

contraction of the lattice may not be the reason for the difference in the coercive field between the thin films and bulk crystals. These variations can be the consequence of lattice imperfections in the thin films.

See supplementary material for more details of the epitaxial representations, ferroelectric measurements, and first-principles calculation.

[1]S. W. Cheong and M. Mostovoy, Nat. Mater. **6**, 13 (2007).

[2]K. F. Wang, J. M. Liu, and Z. F. Ren, Adv. Phys. **58**, 321 (2009).

[3]H. Zheng, J. Wang, S. E. Lofland, Z. Ma, L. Mohaddes-Ardabili, T. Zhao, L. Salamanca-Riba, S. R. Shinde, S. B. Ogale, F. Bai, D. Viehland, Y. Jia, D. G. Schlom, M. Wuttig, A. Roytburd, and R. Ramesh, Science **303**, 661 (2004).

[4]W. Ratcliff, J. W. Lynn, V. Kiryukhin, P. Jain, and M. R. Fitzsimmons, npj Quantum Mater. **1**, 16003 (2016).

[5]W. Eerenstein, N. D. Mathur, and J. F. Scott, Nature **442**, 759 (2006).

[6]N. A. Benedek and C. J. Fennie, Phys. Rev. Lett. **106**, 107204 (2011).

[7]A. B. Harris, Phys. Rev. B **84**, 064116 (2011).

[8]W. Zhu, L. Pi, Y. Huang, S. Tan, and Y. Zhang, Appl. Phys. Lett. **101**, 192407 (2012).

[9]A. T. Mulder, N. A. Benedek, J. M. Rondinelli, and C. J. Fennie, Adv. Funct. Mater. **23**, 4810 (2013).

[10]M. V. Lobanov, M. Greenblatt, El'ad N. Caspi, J. D. Jorgensen, D. V. Sheptyakov, B. H. Toby, C. E. Botez, and P. W. Stephens, J. Phys.: Condens. Matter **16**, 5339 (2004).

[11]S. Dong, J. M. Liu, S. W. Cheong, and Z. Ren, Adv. Phys. **64**, 519 (2015).

[12]E. Bousquet, M. Dawber, N. Stucki, C. Lichtensteiger, P. Hermet, S. Gariglio, J.-M. Triscone, and P. Ghosez, Nature **452**, 732 (2008).

[13]N. A. Benedek, A. T. Mulder, and C. J. Fennie, J. Solid State Chem. **195**, 11 (2012).

[14]M. M. Elcombe, E. H. Kisi, K. D. Hawkins, T. J. White, P. Goodman, and S. Matheson, Acta Crystallogr. B **47**, 305 (1991).

[15]Y. S. Oh, X. Luo, F. T. Huang, Y. Wang, and S. W. Cheong, Nat. Mater. **14**, 407 (2015).

[16]F. T. Huang, F. Xue, B. Gao, L. H. Wang, X. Luo, W. Cai, X. Z. Lu, J. M. Rondinelli, L. Q. Chen, and S. W. Cheong, Nat. Commun. **7**, 11602 (2016).

[17]M. J. Pitcher, P. Mandal, M. S. Dyer, J. Alaria, P. Borisov, H. Niu, J. B. Claridge, and M. J. Rosseinsky, Science **347**, 420 (2015).

[18]C.-H. Lee, N. D. Orloff, T. Birol, Y. Zhu, V. Goian, E. Rocas, R. Haislmaier, E. Vlahos, J. A. Mundy, L. F. Kourkoutis, Y. Nie, M. D. Biegalski, J. Zhang, M. Bernhagen, N. A. Benedek, Y. Kim, J. D. Brock, R. Uecker, X. X. Xi, V. Gopalan, D. Nuzhnyy, S. Kamba, D. A. Muller, I. Takeuchi, J. C. Booth, C. J. Fennie, and D. G. Schlom, Nature **502**, 532 (2013).

[19]X. Z. Lu and J. M. Rondinelli, Nat. Mater. **15**, 951 (2016).

[20]J. Wang, J. B. Neaton, H. Zheng, V. Nagarajan, S. B. Ogale, B. Liu, D. Viehland, V. Vaithyanathan, D. G. Schlom, U. V. Waghmare, N. A. Spaldin, K. M. Rabe, M. Wuttig, and R. Ramesh, Science **299**, 1719 (2003).

[21]G. Catalan and J. F. Scott, Adv. Mater. **21**, 2463 (2009).

[22]C. Lu, W. Hu, Y. Tian, and T. Wu, Appl. Phys. Rev. **2**, 021304 (2015).

[23]M. Nakamura, Y. Tokunaga, M. Kawasaki, and Y. Tokura, Appl. Phys. Lett. **98**, 082902 (2011).

[24]X. Li, C. Lu, J. Dai, S. Dong, Y. Chen, N. Hu, G. Wu, M. Liu, Z. Yan, and J. M. Liu, Sci. Rep. **4**, 7019 (2014).

[25]E. A. Nowadnick and C. J. Fennie, Phys. Rev. B **94**, 104105 (2016).

[26]S. P. Beckman, X. Wang, K. M. Rabe, and D. Vanderbilt, Phys. Rev. B **79**, 144124 (2009).